1 Exploring adsorption of neutral aromatic pollutants onto graphene nanomaterials via 2 molecular dynamics simulations and theoretical linear solvation energy relationships 3 4 Ya Wang, abc Jeffrey Comer, *d Zhongfang Chen, c Jingwen Chen, b James C. Gumbart a 5 6 ^a School of Physics, Georgia Institute of Technology, Atlanta, GA 30332, USA 7 ^b Key Laboratory of Industrial Ecology and Environmental Engineering (MOE), School of Environmental Science and Technology, Dalian University of Technology, Linggong Road 2, 8 9 Dalian 116024, China 10 ^cDepartment of Chemistry, University of Puerto Rico, San Juan, PR 00931, USA 11 d Institute of Computational Comparative Medicine, Nanotechnology Innovation Center of 12 Kansas State, Department of Anatomy and Physiology, Kansas State University, Manhattan, 13 Kansas 66506-5802, USA

Abstract

15

16

17

18

19

20

21

22

23

24

25

26

27

28

29

30

31

32

33

34

Investigation on the adsorption for organic pollutants onto graphene nanomaterials, is not only useful for exploring their potential adsorbent applications, but also helpful for better understanding their fate and evaluating their risks in aquatic environment. Given that the experimental determinations for the adsorption equilibrium coefficients are high workload, time-consuming and expensive, development of prediction models for adsorption onto graphene nanomaterials is becoming an urgent need. Herein molecular dynamics (MD) simulations and theoretical linear solvation energy relationships (TLSERs) were employed to predict the thermodynamics of adsorption for uncharged organic pollutants on graphene and graphene oxides. MD simulations for the adsorption of 43 neutral aromatic compounds onto graphene and diverse models of graphene oxides with various functional groups (hydroxyl, epoxy and carbonyl) demonstrated that graphene has a stronger affinity for the aromatic compounds than graphene oxides. The hydroxyl and carbonyl groups of graphene oxides were found to form hydrogen bonds with the aromatic adsorbates, while epoxy groups did not. Four TLSER models were developed for predicting the adsorption equilibrium coefficients onto graphene and graphene oxide nanosheets. The results showed that dispersion and hydrophobic interactions (V) and H-donating ability (ε_{α}) prevail in the adsorption of uncharged aromatic solutes onto these nanomaterials. These models provide in silico approaches for predicting adsorption affinities onto graphenic nanomaterials.

Environmental significance

35

36

37

38

39

40

41

42

43

44

45

46

47

48

49

50

51

52

Graphene and its derivatives have an extraordinary propensity to accumulate adsorbed organic pollutants, which results in its potential applications as sorption materials in various fields. Meanwhile, the adsorption of organic pollutants on graphenic nanomaterials in aquatic environment can affect their environmental fate and bring potential ecotoxicological risks. Predicting the adsorption equilibrium coefficients and understanding the adsorption mechanisms towards graphenic nanomaterials is helpful for exploring the potential applications for graphene nanomaterials as well as evaluating their environmental risks. In this study, molecular dynamics (MD) simulations were carried out to systematically examine the adsorption behavior of 43 uncharged aromatic pollutants onto graphene and graphene oxides with different functional groups (hydroxyl, epoxy and carbonyl) at an atomic level. The results indicated that the interactions between neutral aromatic compounds and graphene are stronger than those between aromatic compounds and graphene oxides. Moreover, theoretical linear solvation energy relationships (TLSERs) models were first established for predicting the adsorption equilibrium coefficients on graphene and graphene oxides. These prediction models offer promising tools to obtain adsorption affinities onto graphenic materials.

1. Introduction

53

54

55

56

57

58

59

60

61

62

63

64

65

66

67

68

69

70

71

72

73

74

Owing to their unique physicochemical properties, graphene and its derivatives have drawn extensive interest since the discovery of graphene in 2004.^{1,2} Their potential applications in various fields (e.g., material science, medicine and biology, among others)^{3.9} have led to a rapid increase in the production of graphene-based materials, for which the annual production capacity is more than 400 tons in China alone.¹⁰ The market for global graphene products was estimated to be worth US\$ 1.5 million in 2015 and will reach to US\$ 2.1 billion by 2025.11 The ever-increasing studies have exhibited that graphene nanomaterials have shown promising potential as sorption materials for applications in these fields, namely, sample-preparation techniques, catalytic processes and wastewater treatment processes, among others, 12-14 owing to their strong adsorption capability. It is noteworthy that aromatic compounds, and particularly their halogenated derivatives, exhibit high affinities for the surfaces of graphenic materials,15-18 and, coincidently, also constitute major pollutants of concern in natural waters and soils, including organochlorine pesticides¹⁹ and brominated flame retardants. 20 Indeed, analytical chemistry 17 and molecular simulations 21 have demonstrated that graphenic nanomaterials, such as graphene, carbon nanotubes, and their oxidized derivatives, possess exceptionally high affinity for organic pollutants of high concern being compared with non-graphenic adsorbents. The graphene nanomaterials that can be unavoidably released into the aquatic environment during their life cycle, can also adsorb the organic pollutants, thereby altering their environmental behavior, fate as well as toxicity.²² Therefore, it is of great importance to investigate the adsorptions between organic pollutants and graphene nanomaterials, which is not only helpful for exploring their potential

adsorbent applications, but also valuable for knowing more about their fate and risks in aquatic environment.

The adsorption of organic compounds to graphene oxide (GO), has also attracted increasing attention in recent years.²³⁻²⁵ Like graphene, various interactions (i.e., van der Waals forces, hydrophobic interactions, electrostatic interactions, π - π stacking and hydrogen bonding interactions) may be involved in the adsorption processes onto graphene oxide.²⁶ The oxygen-containing functional groups, namely, hydroxyl, epoxy, carbonyl and carboxyl, attached to the basal plane of GO, can affect the interactions between organic compounds and GO. They can also change the hydrophobicity of graphene nanosheets, which affects the interactions between graphene nanosheets and water molecules.²⁷ For example, GO with moderate oxidation has the weakest adsorption capability for nitroaromatic chemicals among these adsorbents, viz., graphene, graphene oxide and reduced graphene oxide.²³ However, there is still a lack of a systematic investigation about the influences of different functional groups attached to GO on the adsorption of diverse sets of organic compounds.

Recently, molecular dynamics (MD) simulation, which can provide an atomic-level view of adsorption, has been used for exploring the interactions between organic compounds and graphene nanomaterials.²⁸⁻³¹ Given numerous organic pollutants detected in the aquatic environment, it is not feasible to simulate the adsorption for compounds onto different graphene nanosheets one by one, even if MD simulation is more efficient than experimental determination. Thus, it is necessary to develop prediction models for estimating adsorption affinities of solutes on graphene and its derivatives.

In our previous study, we developed poly-parameter linear free energy relationships

(pp-LFERs), which are based on Abraham descriptors, for predicting the adsorption energies of organic compounds onto pristine graphene in gaseous and aqueous phases.³² However, these pp-LFERs are only applicable to the compounds having Abraham descriptor values, which are determined experimentally. Emerging pollutants lack these descriptor values, preventing the use of pp-LFERs. Theoretical linear solvation energy relationships (TLSERs), ^{33,34} on the other hand, can be developed using theoretical descriptors from molecular structures, overcoming the limitations of experimental data. Up to now, a TLSER prediction model for graphene has not been established, nor has a model for graphene oxide with different functional groups.

Considering that neutral chemicals generally show higher toxicity than their charged species, 35,36 which indicates that they may have higher environmental risk than the charged ones, in this study, we chose 43 uncharged aromatic organic compounds as adsorbates. Besides, different graphene oxides with functional groups (hydroxyl, epoxy and carbonyl) were built as adsorbents. We systematically explored the adsorption mechanisms of 43 neutral organic compounds onto graphene oxidesby MD simulations. Furthermore, we developed theoretical prediction models for the adsorption equilibrium coefficients onto graphene and graphene oxide nanosheets. These simulations provide insight into the adsorption mechanisms onto graphene oxides. Moreover, the prediction models developed in the current work can serve as an efficient, novel approach to obtain adsorption data for various uncharged compounds toward graphene and graphene oxides.

2. Computational details

2.1. Organic compounds and graphene nanosheet models

Herein, 43 neutral aromatic pollutants, including benzene and its derivatives (Table 1), were chosen as adsorbate models for their ubiquitous existence in natural waters and soils. Moreover, these 43 compounds have diverse functional groups, which is useful for probing the influence of functional groups on adsorption equilibrium coefficients. Their structures were downloaded from ChemSpider 37 and ChemicalBook. 38 These compounds were parameterized according to the CHARMM General Force Field (CGenFF), 39 using the ParamChem Web interface.40,41 Graphene sheet consisting of 160 carbons was built as original small periodic cell. Besides, in order to investigate the effects of functional groups attached to GO on adsorption, we built small periodic patches for graphene oxides sheets, i.e., graphene oxide with hydroxyl groups (GO H), graphene oxide with epoxy groups (GO E) and graphene oxide with carbonyl groups (GO_C), having the same O/C ratio (0.125) which is comparable to the O/C ratio (0.12)²³ in the synthesized GO. The chemical compositions are C₃₂(OH)₄ for GO_H, C₃₂O₄ for GO_E and C₃₂O₄ for GO_C, respectively. We also built a periodic patch for graphene oxide with a mixture of hydroxyl and epoxy groups (GO_M), with a chemical composition of C128O12(OH)24 and an O/C ratio (0.28), which is similar to the experimental O/C ratio (0.30).²³ The size for GO M is three times larger than that for other graphene oxide models. Subsequently, these patches were solvated by adding 60 water molecules, creating an ~30 Å layer of water between periodic images of the graphene sheet. To relax the structures for these graphene nanomaterials and verify their chemical stability, we simulated each solvated structure in a reactive molecular dynamics framework (ReaxFF).42 For each structure, we performed energy minimization and 10 ps of equilibration at a temperature of 300 K and a

119

120

121

122

123

124

125

126

127

128

129

130

131

132

133

134

135

136

137

138

139

pressure of 1 atm, using the ReaxFF implementation⁴³ of LAMMPS.⁴⁴ The parameters for the conventional molecular dynamics simulations were obtained by creating Kekulé representations (where aromatic bonds are represented by a consistent set of single and double bonds) of the structures produced by the ReaxFF energy minimization and submitting the results to the ParamChem web interface.^{40,41} Thereafter, we tiled the periodic structures in the plane of the sheet, and built a $2 \times 2 \times 1$ supercell for GS, a $5 \times 5 \times 1$ supercell for GO_H, a $5 \times 5 \times 1$ supercell for GO_E, a $5 \times 5 \times 1$ supercell for GO_K and a $2 \times 3 \times 1$ supercell for GO_M with the original small patches correspondingly, so that they have similar supercell sizes and are large enough to accurately accommodate adsorption of the solutes.

Note that these graphene and graphene oxides models were not directly parameterized according to CGenFF (CG2R61), for the reason that previous simulations representing graphene by the standard aromatic carbon type of CGenFF (CG2R61) yielded excellent correlation with experiments; however, the adsorption equilibrium constants were underestimated by a factor of about 8.**Error! Bookmark not defined.** To improve agreement with the experiments, we made modifications to the specific Lennard-Jones size parameter (called NBFIX in the CHARMM framework) between sp^2 graphenic carbon atoms and water oxygen atoms. The parameter σ (Cgraph and Owater) was shifted from its original value (0.1031843 kcal/mol) by $j\Delta\sigma$, where j was an integer $-8 \le j \le 8$ and $\Delta\sigma = 0.005$, producing 16 force field variants. The logarithms of the adsorption equilibrium constants (log K) were calculated for four compounds (BzOMe, PhEt, NoT, and PrBn) for each force field variant as described by Comer et al.**Error! Bookmark not defined.** Here, "log" denotes a base-10 logarithm and K has units of mL/g. The variants with j = -2 and -3 gave mean log K values for

the four compounds in the closest agreement with experiment; thus, the calculations for these two variants were extended to 29 aromatic compounds with various physicochemical properties, Error! Bookmark not defined. 45 for which experimental log K values were available and in a range of 1.96 ~ 5.68. The variant j = -3 yielded the best agreement with experiment, having a mean log K of 3.69 over all 29 compounds, similar to the mean of the experimental values, 3.66. In addition to the reduced mean deviation from experiment in comparison to the standard CGenFF parameters, this force field variant also yielded improved correlation with experiment: r = 0.920. Hence, all simulations were performed with σ (Cgraph and Owater) = 0.0881843 kcal/mol. Since this special Lennard-Jones parameter was parameterized to represent graphene-like carbon, it applied only to sp^2 carbon atoms in the graphene oxide structures (sp^3 atoms retained standard parameters).

Subsequently, molecular dynamics simulations without imposing constraints on the supercells, were carried out using the software NAMD 2.12.46 The final size of the simulation cell for system including graphene and compounds was 39.1 Å × 42.3 Å × 39.3 Å. The sizes of supercells for systems including graphene oxides and chemicals were 49.3 Å × 42.6 Å × 41.6 Å (GO_H), 50.4 Å × 43.8 Å × 39.2 Å (GO_E), 48.9 Å × 43.2 Å × 41.0 Å (GO_C) and 40.2 Å × 51.9 Å × 40.4 Å (GO_M). More details about adsorbent models are provided in Fig. 1.

Table 1. Organic Compounds and Logarithm Values of Calculated Adsorption Equilibrium

		Substituents	log K_calculated				
No	Compound		GO GO				
•	-		GS	GO_H	GO_E	C	M
1	benzene (PhH)		1.70	0.93	1.56	1.68	0.13
2	chlorobenzene (PhCl)	-Cl	2.92	1.56	2.49	2.54	0.82
3	bromobenzene (PhBr)	-Br	2.81	1.23	2.31	2.73	0.95
4	iodobenzene (PhI)	-I	3.26	1.56	2.49	2.84	0.79
5	phenol (PhOH)	-OH	2.65	1.37	2.04	2.33	0.89
6	benzonitrile (PhCN)	-CN	3.55	1.82	2.64	2.46	0.92
7	nitrobenzene (PhNO2)	-NO ₂	3.99	2.16	2.66	2.62	1.90
8	toluene (PhMe)	-CH ₃	2.67	1.10	1.97	2.13	0.21
9	phenylmethanol (PhMl)	-CH ₂ OH	2.52	1.76	2.10	2.09	0.93
10	ethylbenzene (PhEt)	-CH ₂ CH ₃	2.73	1.49	2.30	2.55	0.87
11	propylbenzene (PhPr)	-CH ₂ CH ₂ CH ₃	3.21	1.69	2.60	2.90	0.76
12	acetophenone (BzMe)	-C(O)CH3	3.91	1.38	2.49	2.68	1.52
13	methylbenzoate (BzOMe)	-C(O)OCH3	4.96	1.62	3.79	3.70	2.06
14	2-phenylethanol (PhEl)	-CH ₂ CH ₂ OH	2.97	1.47	2.53	2.67	1.04
15	phenylacetate (PhOAc)	-OC(O)CH3	3.08	1.69	2.22	2.55	0.92
16	ethylbenzoate (BzOEt)	-C(O)OCH ₂ CH	5.45	1.97	3.68	3.93	2.30
		3					
17	4-fluorophenol (FPI)	-OH, -F	3.09	1.56	2.38	2.50	0.77
18	3-chlorophenol (ClPl)	-OH, -Cl	3.62	1.86	2.70	3.33	1.27
19	3-bromophenol (BrPl)	-OH, -Br	4.01	1.68	3.19	3.43	1.62
20	m-cresol (mCr)	-OH, -CH3	3.30	1.50	3.06	3.01	1.18
21	p-cresol (PCRO)	-CH3, -OH	3.63	1.41	2.85	3.21	1.42
22	4-ethylphenol (EPHE)	-OH, -CH ₂ CH ₃	3.65	1.78	3.02	3.25	0.95
23	p-xylene (PXYL)	-CH ₃	3.66	1.47	2.83	2.97	1.35
24	4-chlorotoluene (PCLT)	-CH ₃ , -Cl	3.58	1.70	3.18	3.09	1.61
25	4-nitrotoluene (NoT)	-NO ₂ , -CH ₃	5.05	1.73	3.50	3.39	2.73
26	(3-methylphenyl) methanol (MeBl)	-CH ₃ , -CH ₂ OH	3.50	1.86	2.72	2.49	1.37
27	4-chloroanisole (ClAn)	-Cl, -OCH3	4.19	2.32	2.95	3.04	1.95
28	4-chloroacetophenone	-Cl, -C(O)CH ₃	4.79	1.99	3.48	3.18	2.05
20	(ClAh)	-Ci, -C(O)Ci is	4.77	1.77	3.40	5.10	2.00
29	1,3-dinitrobenzene (DNIN)	-NO ₂	5.76	2.28	3.04	2.75	3.02
30	methyl 2-methyl benzoate	-CH ₃ ,	5.13	1.52	3.84	3.64	2.22
	(MMBa)	-C(O)OCH3					
31	4-chloroaniline (PhAm)	-Cl, -NH ₂	3.12	1.60	2.32	2.72	1.50
32	3,5-dimethylphenol (dMPl)	-OH, -CH₃	4.50	1.14	3.65	3.23	2.13
33	hexabromobenzene (HBB)	-Br	9.52	1.82	5.85	4.68	4.24
34	pentabromotoluene (PBT)	-Br, -CH ₃	9.55	1.95	6.37	4.62	4.92
35	1,2-dibromo-4-(1,2-dibromo	-Br,	5.87	2.66	3.95	3.68	2.05

	ethyl)-cyclohexane (TBE)	-CHBrCH ₂ Br					
36	tetrabromo-o-chlorotoluene	-Cl, -Br, -CH ₃	9.08	1.96	5.85	4.10	5.05
	(TBCT)						
37	naphthalene (NAFT)		4.26	1.33	4.14	4.20	2.22
38	biphenyl (PhPh)		5.09	2.11	4.67	4.68	2.71
39	1-methylnaphthalene -CH ₃		5.21	1.73	4.92	4.41	2.60
	(MeNh)						
40	BDE209 (B209)	-O-, -Br	9.65	2.32	5.85	5.27	2.59
41	BDE47 (B47)	-O-, -Br	5.85	3.83	4.13	4.41	2.63
42	BDE99 (B99)	-O-, -Br	6.06	3.92	5.00	5.21	4.22
43	BDE207 (B207)	-O-, -Br	9.39	4.06	5.63	4.28	5.12

GS: graphene sheet; GO_H: graphene oxide with hydroxyl groups; GO_E: graphene oxide with epoxy groups; GO_C: graphene oxide with carbonyl groups; GO_M: graphene oxide with mixed hydroxyl and epoxy groups.

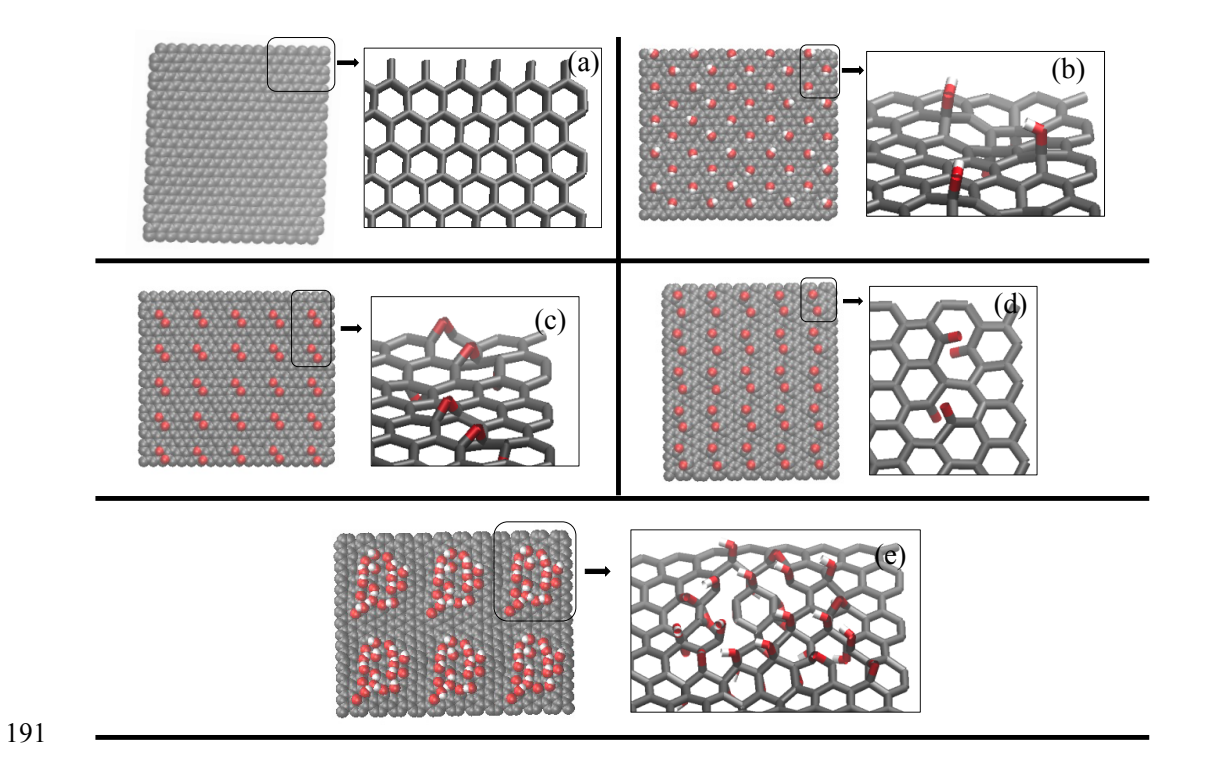


Fig. 1 The structures for graphene and graphene oxides. (a) graphene (GS); (b) graphene oxide with hydroxyl groups (GO_H); (c) graphene oxide with epoxy groups (GO_E); (d) graphene oxide with carbonyl groups (GO_C); (e) graphene oxide with a mix of hydroxyl and epoxy groups (GO_M).

2.2. Molecular dynamics simulations

All the molecular dynamics simulations for the systems including graphene nanomaterials and each aromatic compound, were performed with NAMD 2.12. The TIP3P water model,⁴⁷ an all-atom explicit-solvent model typically used with the CHARMM force field, was used for simulating the aqueous environment. The temperature and pressure were set 300 K and 1 atm, by using Langevin thermostat and Langevin piston methods ⁴⁸ respectively. A timestep of 2 fs was set for bonded interactions and short-range non-bonded interactions. The cut-off was set at 9 Å; the particle-mesh Ewald algorithm⁴⁹ was employed to treat the long-range electrostatic interactions every other time step. Analyses were performed with VMD 1.9.3.⁵⁰

2.3. Calculation of adsorption equilibrium coefficients (K)

Every system underwent 2000 steps of energy minimization before the calculation of free energies, which were obtained with the adaptive biasing force (ABF)^{51,52} method. The Colvars module⁵³ of NAMD 2.12 was used to implement ABF along the z component of the vector between the center of mass for the organic compounds and the center of mass for the graphene or graphene oxide nanosheets. All the calculations were performed using a window with an interval $3 \le z \le 15$ Å, and the forces were sampled in bins with a width of 0.05 Å. Each simulation was run for 50 ns. To verify convergence of the free energy, a few systems were run for an additional 50 ns and no significant change was observed. The potentials of mean force from the 50 ns simulations were normalized so that the mean value on $14 \le z \le 15$ Å was zero.

The adsorption equilibrium coefficients can be estimated with the method defined by

219 Comer et al.:Error! Bookmark not defined.

$$K^{\text{calc}} = \frac{\sigma}{M} \int_0^c dz \, e^{-\beta W^{\text{calc}}(z)} \tag{1}$$

- where $\beta = (k_B T)^{-1}$ represents the reciprocal thermal energy, and $W^{\text{calc}}(z)$ is the potential of mean
- force calculated by ABF. σ/M denotes the specific surface areas of the graphene nanomaterials.
- Here, the experimentally measured K values by Brunauer-Emmett-Teller method,²³ 298.8 m²/g
- for GS, GO_H, GO_E and GO_C, and 7.707 m²/g for GO_M, are used to compare with our
- simulation results.

226

227

228

229

230

231

232

233

234

235

236

238

239

2.4. Theoretical descriptors for prediction models

All the molecules were optimized at the M06-2X/6-31G(d, p) ⁵⁴ level using the GAUSSIAN 09 program unless stated otherwise. ⁵⁵ The LANL2DZ basis set ⁵⁶ was used for Br and I atoms. All the optimized structures were confirmed to be local minima by vibrational frequency analyses. Quantum chemical descriptors, including molecular polarizability, atomic charges, the highest occupied molecular orbital energy level (*E*_{LUMO}) and the lowest unoccupied molecular orbital energy level (*E*_{LUMO}) values, were extracted from the Gaussian output files. McGowan volumes were generated by using Dragon software ⁵⁷ with the optimized structures. According to theoretical linear solvation energy relationships, ^{58,59} we used six theoretical descriptors for developing prediction models, which can be expressed as follows:

$$\log K = a\varepsilon_{\alpha} + b\varepsilon_{\beta} + fq^{+} + eq^{-} + vV + p\pi + g \tag{2}$$

where log K represents logarithm of the experimentally determined adsorption equilibrium constant; ε_{α} (E_{LUMO} – $E_{\text{HOMO(water)}}$), in an energy unit of electron volt (eV), is defined as covalent

acidity; $\varepsilon_{\beta}(E_{\text{LUMO(water)}} - E_{\text{HOMO}})$ in eV, is covalent basicity; q^{+} , the most positive formal charge on a hydrogen atom in the molecule in atomic charge unit (acu), is taken as electrostatic acidity; likewise, q^{-} (acu), the absolute value of the most negative formal charge in the molecule, represents the electrostatic basicity; V is obtained by dividing the molecular volume (V_x , in mL/mol) by 100; π , a unitless quantity, is calculated by dividing the polarizability by V. a, b, f, e, v and p are fitting coefficients, and g is a regression constant. $a\varepsilon_{\alpha}$, $b\varepsilon_{\beta}$, eq^{-} and fq^{+} describe the hydrogen bonding terms; vV characterizes bulk/cavity term; and $p\pi$ is the dipolarity/polarizability term. By convention, the logarithm in equation (2) is base-10 and the K has units of mL/g.

2.5. Models development and characterization

The calculated log K values for 43 organic compounds were used for establishing prediction models. Besides, we also randomly split the total 43 organic compounds into a training set of 35 aromatic compounds and a validation set of 8 aromatic compounds (Table S1 of the Supplementary Information, SI), and developed prediction models with the training set. Four parameters, namely, the determination coefficient (R^2), root mean square error (RMSE), leave-one-out cross-validated Q^2 (Q^2LOO), and Q^2 from bootstrap resampling (Q^2ROOT) (1/5, 5000 iterations), were used to evaluate the goodness of fit and robustness. Additionally, the application domain (AD) of the prediction models was characterized with a Williams plot, which is based on standardized residuals (δ^2) and leverage values (h_1).

3. Results and discussion

3.1. log K values for organic compounds on graphene and graphene oxides

Experimental log K values are available for three of the compounds examined in this

study, namely 1, 3-dinitrobenzene (DNIN), 4-nitrotoluene (NoT) and nitrobenzene (PhNO2).²³ Table 2 compares our calculated log *K* values with the experimental ones. The mean absolute errors are 0.51 and 0.24 for GS and GO_M, respectively, indicating that molecular dynamics simulation is a viable alternative method for getting log *K* values for adsorption onto graphene nanomaterials.

Table 2. The Experimental and Calculated log K Values for DNIN, NoT and PhNO2 on GS

269 and GO_M

Commound	log K on	GS	log K on GO_M		
Compound	Experimental*	Calculated	Experimental*	Calculated	
DNIN	5.82	5.76	2.59	3.02	
NoT	4.91	5.05	2.79	2.73	
PhNO2	5.31	3.99	2.14	1.90	

* The experimental log *K* values are obtained from Chen *et al.*'s studies.²³

Table 1 lists the categories of functional groups for 43 organic compounds and the calculated log *K* values on graphene and graphene oxides. The log *K* values (Fig. 2) in simulations on unmodified graphene are in the range of 1.70 to 9.65, which is wider than the ranges for graphene oxides, i.e., 0.93 to 4.06 (GO_H), 1.56 to 6.37 (GO_E), 1.68 to 5.27 (GO_C) and 0.13 to 5.12 (GO_M). The log *K* values for organic compounds on graphene are larger than those on graphene oxides, namely, GO_H, GO_E and GO_C, which implies that graphene has a stronger adsorption capability than graphene oxides.

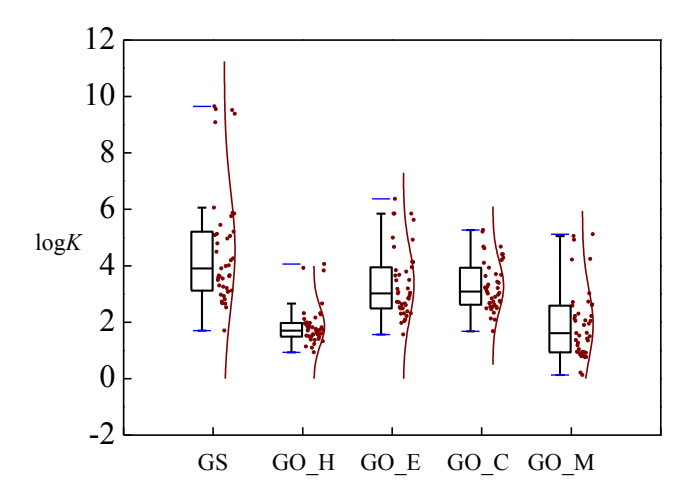


Fig. 2 Whisker and box plot representation of the log *K* values on GS, GO_H, GO_E, GO_C and GO_M. The blue lines above and below the rectangles in the plot represent the maximum and minimum log *K* values on each graphene nanosheet; the top and the bottom of the rectangles represent the 75th and 25th percentiles, respectively; the lines within the rectangles represent 50th percentiles.

3.2. The influence of hydroxyl, epoxy and carbonyl groups for adsorption on graphene oxides

The calculated free energy varies with changing the distance (*r*) between the center of mass for organic compounds and the surface for graphene and its oxides (Fig. 3 and Fig. S1). Moreover, similar trends were observed in the changes of free energy for 43 compounds on different graphene nanomaterials. In order to explore the effect of hydroxyl, epoxy and carbonyl groups on the adsorption, we focus the discussion on the free energies for the systems including six most representative aromatic compounds, namely, PhH, PhMe, PhOH, PhCN, PhCl and PhNO2 (Fig. 3). For GS, the free energies for organic compounds at the bottom of each valley are -4.58 kcal/mol (PhH), -5.91 kcal/mol (PhMe), -5.93 kcal/mol

(PhOH), -7.20 kcal/mol (PhCN), -6.29 kcal/mol (PhCl), and -7.78 kcal/mol (PhNO2). All these values are lower than those on graphene oxides. This further demonstrates that the graphene has the strongest adsorption affinity for these model adsorbates. For GO_H, the free energies for these adsorbates at the bottom of each valley are -3.31 kcal/mol (PhH), -3.53 kcal/mol (PhMe), -3.98 kcal/mol (PhOH), -4.67 kcal/mol (PhCN), -4.28 kcal/mol (PhCl), and -5.12 kcal/mol (PhNO2), and these values are less favorable than those on the other GO models. Thus, graphene oxide with hydroxyl groups has weaker adsorption affinity than the graphene oxides with other functional groups. Note that the bottom of each valley for free energies on GO_H in Fig. 3 locates at ca. 3.8 Å, while it locates at ca. 3.5 Å for the free energies on GS, which may be understood by the fact that steric effects for hydroxyl groups on GO_H hinder the adsorbates from approaching GO_H.

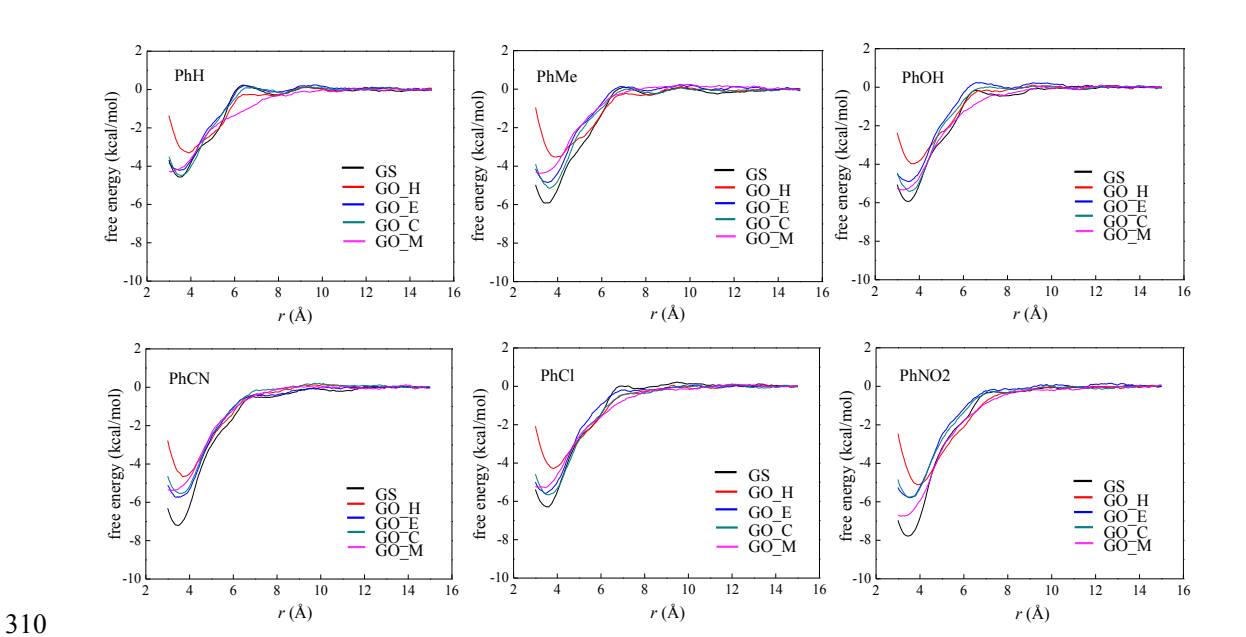


Fig. 3 Calculated free energy versus distance (*r*) between the center-of-mass for six organic compounds and the surface of graphene or graphene oxide nanosheets.

Furthermore, we calculated radial distribution functions (RDFs) for electron-withdrawing atoms (i.e., N, O, F, Cl, Br, I) in a compound relative to the hydrogen atom in hydroxyl groups on GO_H (Fig. 4). The electron-withdrawing atoms in these compounds, namely chlorobenzene (PhCl), bromobenzene (PhBr), iodobenzene (PhI), phenol (PhOH) and benzonitrile (PhCN), tend to distribute closer to the H atoms on GO_H, as compared to the compound, indicating that there exists electrostatic interactions between these electron-withdrawing atoms and H atoms. Especially for N and O atoms, g(r) has a peak at ca. 2 Å, which is within the range of hydrogen bonding interactions. Thus, electrostatic interactions play important roles in adsorption of organic compounds with electron-withdrawing atoms on GO_H, while for compounds with N or O atoms, hydrogen bonding interactions also contribute to the adsorption onto GO_H. In addition, we also calculated g(r) for H atoms in the substituent of a compound relative to the O atoms in hydroxyl groups of GO_H. The RDFs (Fig. 4) for toluene (PhMe), ethylbenzene (PhEt), and propylbenzene (PhPr) indicate that there are no hydrogen bonding interactions between the H atoms of -CH₂, -CH₂CH₃ and -CH₂CH₂CH₃ functional groups and the O atoms of GO_H. The g(r) values for PhOH, 4-fluorophenol (FPl), 3-chlorophenol (ClPl) and phenylmethanol (PhMl), however, have a peak at around 2 Å, implying that hydrogen bonds exist between the hydrogen atom in -OH groups of these four compounds and the O atoms of GO_H. Note that CIPI acts as a hydrogen bond donor and acceptor to -OH group on the GO_H, while 3-bromophenol (BrPl) acts only as a hydrogen bond acceptor. Likewise, m-cresol (mCr) and p-cresol (PCRO) act as hydrogen bond acceptors, though the hydroxyl group in PhOH tends to be a hydrogen bond donor. Therefore, the substituent in a phenol

314

315

316

317

318

319

320

321

322

323

324

325

326

327

328

329

330

331

332

333

334

can affect the formation of hydrogen bonds between the –OH and the GO_H. Moreover, RDFs for methylbenzoate (BzOMe) and phenylacetate (PhOAc) in Fig. 4 show that BzOMe has a greater propensity to form hydrogen bonds than PhOAc, even though their structures are similar. The reason may be that the oxygen atom in C=O for BzOMe maintaining the conjugation is richer in electrons than the oxygen atom in C=O for PhOAc, and prefers to act as a hydrogen bond acceptor.



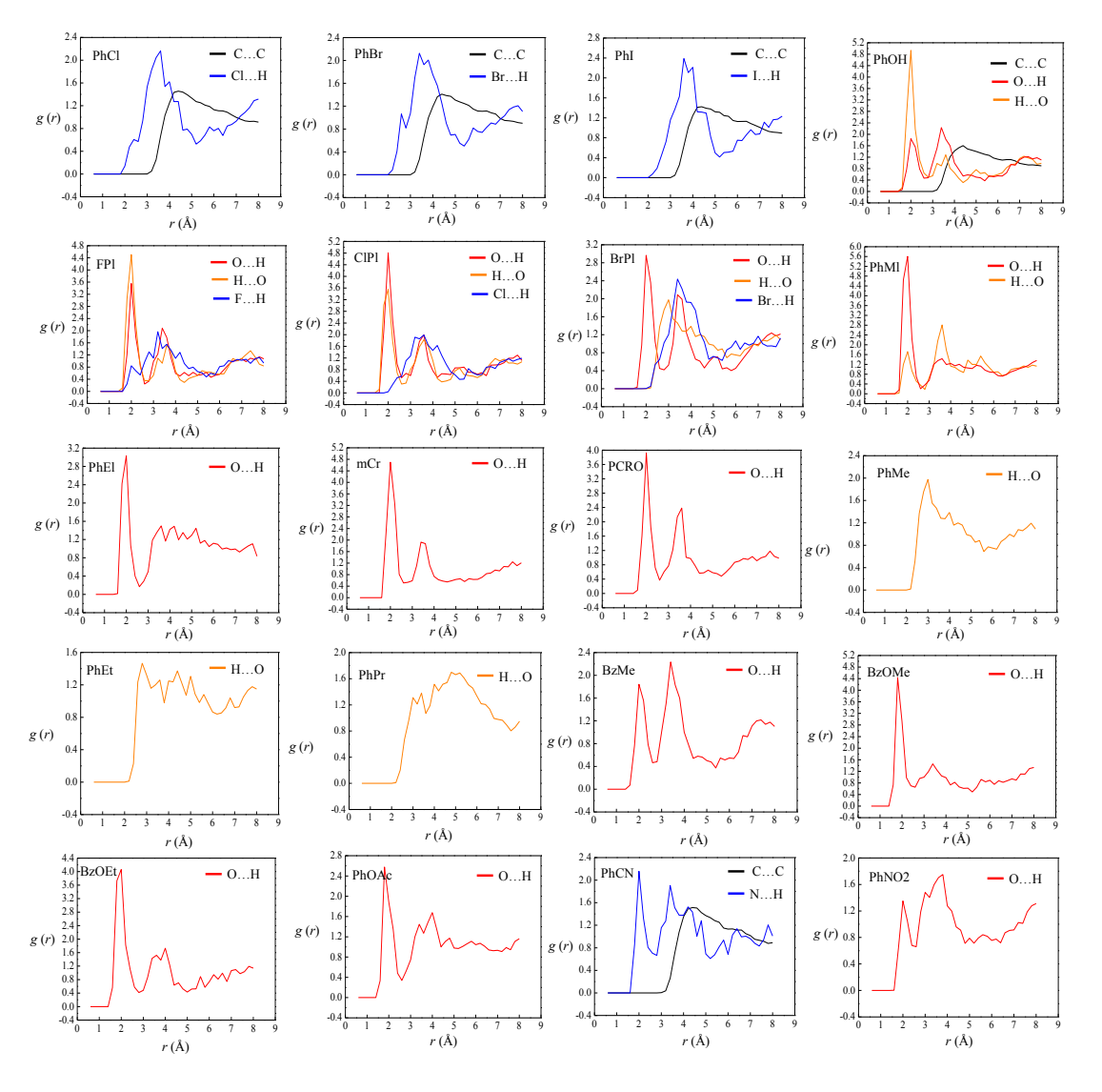


Fig. 4 RDFs for compounds relative to GO_H. C...C: RDFs for all carbon atoms in a compound relative to the graphene nanosheet; H...O: RDFs for H in the substituent of a

compound relative to O in the hydroxyl group on GO_H; N...H: RDFs for N in the substituent of a compound relative to H in the hydroxyl group; O...H, F...H, Cl...H, Br...H and I...H were defined similarly.

For graphene oxide with epoxy groups (GO_E), we also examined the RDFs for different atoms, i.e., H atoms in the functional groups –OH, –CH₃, –CH₂CH₃ and –CH₂CH₂CH₃ as well as N atoms in –CN, relative to the O atom in epoxy functional groups (see Fig. S2). None of the RDFs exhibit a peak at ca. 2 Å, indicating that no hydrogen bonds exist between the inspected organic chemicals and the GO_E nanosheet. Similarly, as for graphene oxide with carbonyl groups (GO_C), the RDFs (Fig. S3) for H atoms in the –OH groups of compounds relative to the O atom on GO_C exhibit a peak at around 2 Å, which reveals that the hydrogen bonding interactions play roles in the adsorption for those compounds having –OH onto GO_C.

As noted above, steric effects result in considerably weaker adsorption for the organic compounds on graphene oxide with hydroxyl groups compared to pristine graphene nanosheets. Graphene oxides with hydroxyl or carbonyl groups can form hydrogen bonds with the –OH group(s) in a compound. The hydroxyl groups in GO_H can also interact with the functional groups, namely, –CH2OH, –C(O)CH3, –C(O)OCH3, –CH2CH2OH, –OC(O)CH3, – C(O)OCH2CH3 and –CN via hydrogen bonding. Moreover, the functional group in phenol can affect its hydrogen bonding between its –OH and GO_H.

3.3. Prediction models for adsorption on GS and on GO_M

The optimal models for predicting log K values of organic compounds onto GS and

- 368 GO_M, which were developed with log *K* values for 43 compounds, are as follows.
- 369 For GS:

$$\log K = -1.826\varepsilon_{\alpha} - 1.297\varepsilon_{\beta} + 0.475q^{+} - 0.937q^{-} + 1.012V - 1.599\pi + 43.011$$
 (3)

371
$$n = 43$$
, $R^2 = 0.881$, $RMSE = 0.703$, $Q^2LOO = 0.827$, $Q^2BOOT = 0.754$

372 For GO_M:

379

goodness-of-fit and robustness.

$$log K = -1.14 ε_α - 0.623 ε_β + 3.519 q^+ - 1.234 q^- + 0.442V + 0.401 π + 17.919$$
 (4)

374
$$n = 43$$
, $R^2 = 0.768$, $RMSE = 0.595$, $Q^2_{LOO} = 0.601$, $Q^2_{BOOT} = 0.752$

Fig. 5(a) shows that the predicted log K values on graphene nanosheets agree well with those determined by MD simulations. Similarly, the predicted log K values on GO_M are in good agreement with those from simulations (Fig. 5(b)). The values for R^2_{adj} ($R^2 > 0.60$), Q^2_{LOO} and Q^2_{BOOT} ($Q^2 > 0.50$), e^{60} and e^{60} and e^{60} indicate that these two models have excellent

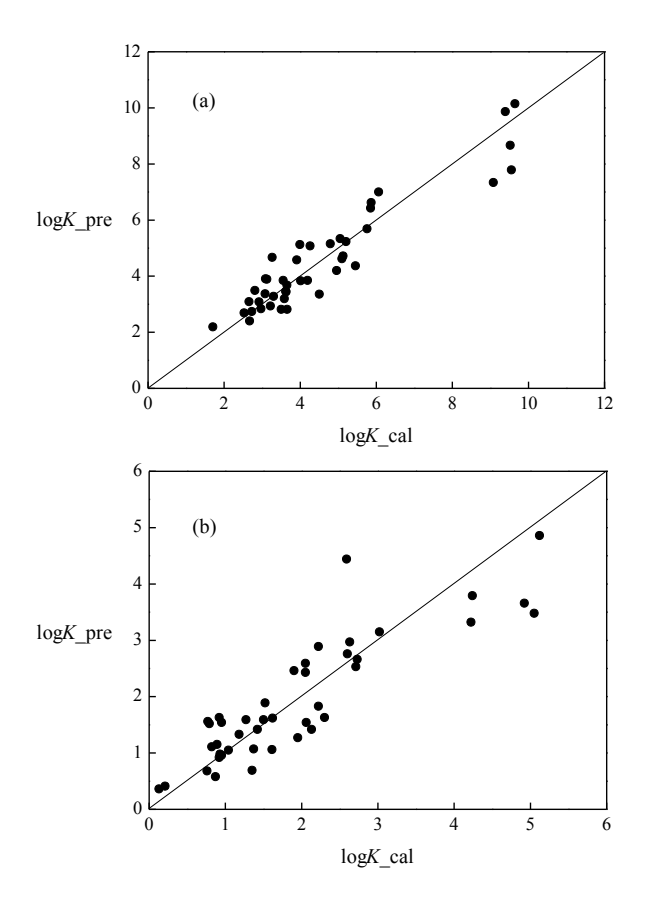


Fig. 5 Predicted log *K* values (log *K*_pre) versus MD calculated ones (log *K*_cal) on (a) GS (Eq. 3) and (b) GO_M (Eq. 4)

Applicability domains of the prediction models (Eq. 3 and Eq. 4) are visualized in Fig. 6. All the compounds have $|\delta^*| < 3$, which shows that there are no outliers. Eq. 3 can be used for predicting log K values onto graphene nanosheets for various aromatic compounds including benzene, alcohols, phenols, anilines, nitrobenzenes, nitriles, halogenated benzenes, ketones, esters, biphenyls, polycyclic aromatic hydrocarbons (PAHs) and polybrominated diphenyl ethers (PBDEs). Eq. 4, with the same applicability domain as Eq. 3, can predict adsorption onto graphene oxide.

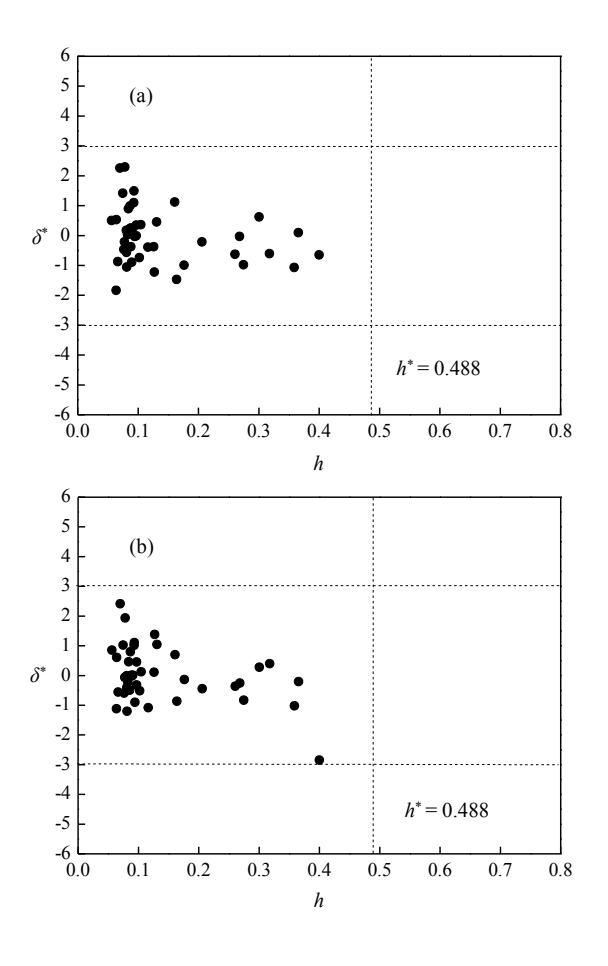


Fig. 6 Williams plot of standardized residuals (δ^*) versus leverages (h) on (a) GS (Eq. 3) and (b) GO_M (Eq. 4)

Furthermore, we established two models (Eq. S1 and Eq. S2) with the training set consisting of 35 organic chemicals. These two developed models (Eq. S1 and Eq. S2) have fitting coefficients (i.e., a, b, f, e, v and p) and regression constant g similar to those in Eq. 3 and Eq. 4. In terms of goodness-of-fit (Table 3), Eq. 3 and Eq. 4 have smaller root mean square errors than those for Eq. S1 and Eq. S2, although the R^2 values for Eq. 3 and Eq. 4 are slightly lower than those for Eq. S1 and Eq. S2. For robustness, the two models (Eq. 3 and Eq. 4) being developed on 43 aromatic compounds perform better than the models (Eq. S1 and Eq. S2) with 35 compounds. Moreover, the chemical domain for the models with whole dataset is

wider than that for those with sub-dataset. More details about the prediction models being based on 35 aromatic compounds can be found in SI. Note that these four prediction models are the first theoretical linear solvation energy relationship models for adsorption onto graphene and graphene oxide.

Table 3. Comparisons of goodness-of-fit, robustness and predictivity ability for the

d	leve	loped	mod	els

		Goodness-of-fit		Robustness		Predictivity
Model	n					ability
		R^2	RMSET	Q^2 LOO	Q^{2} boot	$RMSE_{ m v}$
GS (Eq. 3)	43	0.881	0.703	0.827	0.754	
GS (Eq. S1)	35	0.882	0.742	0.818	0.712	0.540
GO_M (Eq. 4)	43	0.768	0.595	0.601	0.752	
GO_M (Eq. S2)	35	0.774	0.621	0.584	0.709	0.525

3.4. Adsorption mechanisms on GS and GO_M

As given in the two prediction models Eq. 3 and Eq. 4, the six terms $a\varepsilon_{\alpha}$, $b\varepsilon_{\beta}$, eq^{-} , fq^{+} , vV and $p\pi$ have different contributions to the log K values. This difference indicates that hydrogen bonding, dispersion, hydrophobic and electrostatic interactions play diverse roles in the adsorption of organic compounds onto graphene and graphene oxide.

For adsorption on graphene (Eq. 3), the covalent acidity (ε_{α}) of the examined organic compounds has a negative contribution to the log K values, indicating that compounds with strong H-donating abilities prefer to form hydrogen bonds with the oxygen atoms in water molecules, leading to a decrease in log K. Similarly, the log K values increase with decreasing covalent basicity (ε_{β}), as compounds with strong H-accepting abilities can interact with the hydrogen atoms in the water molecules as H-acceptors. Electrostatic acidity (q^{+}) has a positive

correlation with the log K values because the hydrogen atom with the most positive formal charge can interact with π electrons around graphene, promoting adsorption of organic compounds onto graphene. On the contrary, the electrostatic basicity (q^-) of a molecule correlates negatively with the log K values.

The term vV, which represents the dispersion and hydrophobic interactions, has a positive contribution to the log K values. In previous prediction models for multiwalled carbon nanotubes, Error! Bookmark not defined. 61 which are based on experimental adsorption data, vV plays an analogous role. Note that the dipolarity/polarizability term $(p\pi)$ negatively correlates with the log K values, indicating that compounds possessing larger polarizability tend to interact with water molecules rather than with graphene.

For adsorption onto graphene oxide (Eq. 4), the terms $a\epsilon_{\alpha}$, $b\epsilon_{\beta}$ and eq^- contribute negatively, while the electrostatic acidity (fq^+) and bulk/cavity (vV) terms are positively correlated with the log K values, similar to those in the graphene prediction model. However, the dipolarity/polarizability ($p\pi$) term makes a positive contribution to the adsorption for organic compounds on graphene oxide, in contrast to graphene. The reason may be that the hydroxyl and epoxy groups in graphene oxide result in polar surface, which promotes stronger interactions with polarizable compounds. To confirm the above reasoning, we computed the electrostatic potential for graphene and graphene oxide with density functional theory, as detailed in the SI. The electrostatic potential around hydroxyl and epoxy groups are negative (Fig. 7), which differs significantly from that on a graphene nanosheet. This demonstrates that the hydroxyl and epoxy groups on graphene oxide increase the polarity of graphene oxide.



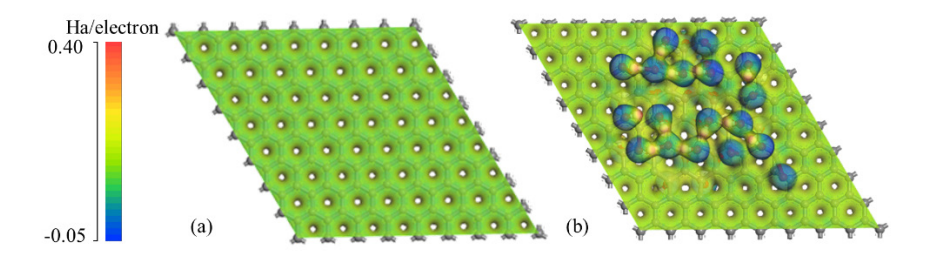


Fig. 7 Electrostatic potential distribution of (a) graphene and (b) GO_M.

Finally, we calculated the Pearson's correlation coefficients (PCCs) to evaluate the influences of the six descriptors used on log K values. As shown in Table 3, the PCCs for ε_{α} and V have the largest magnitudes in both graphene and graphene oxide models: in the graphene prediction model, they are -0.826 and 0.831, respectively, while for the graphene oxide model, they are -0.776 and 0.711 (Table 4). Thus, for both graphene and graphene oxide, the H-donating ability (ε_{α}) and dispersion/hydrophobic interactions (V) are the most influential factors on the partitioning of organic compounds between graphene nanosheets and water.

Table 4. Descriptors and Their Pearson's Correlation Coefficients (PCCs)

Descriptor	PCCs (GS)	PCCs (GO_M)
\mathcal{E}_{α}	-0.826	-0.776
$oldsymbol{arepsilon}eta$	0.369	0.313
q^-	-0.063	-0.066
$q^{\scriptscriptstyle +}$	-0.422	-0.300
V	0.831	0.711
π	0.253	0.366

 PCCs (GS): Pearson's correlation coefficients for the descriptors in the graphene prediction model; PCCs (GO_M): Pearson's correlation coefficients for the descriptors in the graphene oxide prediction model.

4. Conclusions

By combining MD simulations and TLSERs, we investigated the adsorption of 43 aromatic solutes on graphene and graphene oxides with the functional groups hydroxyl, epoxy and carbonyl. MD simulations provided us an atomic-level view of the adsorption process and an in-depth understanding of how different functional groups attached to the graphene nanosheet influence adsorption from aqueous solution. The results illustrate that the hydroxyl and carbonyl groups on graphene oxides can form hydrogen bonds with a solute's –OH group, while the epoxy group does not form hydrogen bonds with the same compound. The newly established TLSER models can enable us to obtain the adsorption data for a much wider range of uncharged compounds onto graphene nanomaterials than the 43 tested ones in this work. This study provides us novel tools to rapidly predict adsorption affinities onto graphene and graphene oxides using only theoretical molecular descriptors, which can overcome the lack of experimental descriptors.

Supplementary information

Electronic supplementary information (ESI) is available: (1) 35 compounds in the training set and 8 compounds in the validation set (Table S1); (2) Calculated free energy versus distance (*r*) between the center-of-mass for 37 organic compounds and the surface of graphene or graphene oxide nanosheets (Fig. S1); (3) Radial distribution functions on GO_E (Fig. S2); (4) Radial distribution functions on GO_C (Fig. S3); (5) Details for prediction models being based on 35 aromatic compounds (SI1); (6) Details for computing the electrostatic potential distribution with density functional theory (DFT) method (SI2).

486 Corresponding Authors

- *James C. Gumbart, Phone: +1-404-385-0797, e-mail: gumbart@physics.gatech.edu.
- *Jeffrey Comer, Phone/fax: +1-785-532-6311, e-mail: jeffcomer@ksu.edu.
- *Jingwen Chen, Phone/fax: +86-411-84706269, e-mail: jwchen@dlut.edu.cn.
- 490 Notes
- 491 The authors declare no competing financial interest.

492 Acknowledgements

- The study was supported in USA by NSF (Grant No. HRD-1736093 to ZC; MCB-1452464 to
- 494 JCG; CHE-1726332 to JC) and NASA (Grant No. 17-EPSCoRProp-0032) and in China by the
- 495 National Natural Science Foundation of China (21325729, 21661142001). Ya Wang
- 496 acknowledges a fellowship from the China Scholarship Council. This work used the Extreme
- 497 Science and Engineering Discovery Environment (XSEDE), which is supported by National
- 498 Science Foundation grant number ACI-1548562.

499 References

- 1 K. S. Novoselov, A. K. Geim, S. V. Morozov, D. Jiang, Y. Zhang, S. V. Dubonos, I. V. Grigorieva and A. A. Firsov, Electric field effect in atomically thin carbon films, *Science*, **2004**, 306, 666–669.
- 2 Y. Shen, Q. L. Fang and B. L. Chen, Environmental applications of three-dimensional graphene-based macrostructures: Adsorption, transformation, and detection, *Environ. Sci. Technol.*, **2015**, 49, 67–84.

- 3 M. L. Pan, Y. Y. Zhang, C. Shan, X. L. Zhang, G. D. Gao and B. C. Pan, Flat graphene-enhanced electron transfer involved in redox reactions, *Environ. Sci. Technol.*, **2017**, 51, 8597–8605.
- 4 A. Ambrosi, C. K. Chua, A. Bonanni and M. Pumera, Electrochemistry of graphene and related materials, *Chem. Rev.*, **2014**, 114, 7150–7188.
- 5 C. Finnerty, L.Zhang, D. L.Sedlak, K. L.Nelson and B. X. Mi, Synthetic graphene oxide leaf for solar desalination with zero liquid discharge, *Environ. Sci. Technol.*, **2017**, 51, 11701–11709.
- 6 S. Navalon, A. Dhakshinamoorthy, M. Alvaro and H. Garcia, Carbocatalysis by graphene-based materials, *Chem. Rev.*, **2014**, 114, 6179–6212.
- 7 K. S. Novoselov, V. I. Fal'ko, L. Colombo, P. R. Gellert, M. G. Schwab and K. Kim, A roadmap for graphene, *Nature*, **2012**, 490, 192–200.
- 8 K. P. Loh, Q. L. Bao, G. Eda and M. Chhowalla, Graphene oxide as a chemically tunable platform for optical applications, *Nat. Chem.*, **2010**, 2, 1015–1024.
- 9 A. Zurutuza and C. Marinelli, Challenges and opportunities in graphene commercialization, *Nat. Nanotechnol.*, **2014**, 9, 730–734.
- 10 W. C. Ren and H. M. Cheng, The global growth of graphene, *Nat. Nanotechnol.*, **2014**, 9, 726–730.
- 11 *Graphene: Technologies, Applications and Markets*; BCC research, 2016; https://www.bccresearch.com/market-research/advanced-materials/graphene-technologies-applications-markets-report-avm075d.html.

- ¹² Q. Liu, J. B. Shi, J. T. Sun, T. Wang, L. X. Zeng and G. B. Jiang, Graphene and graphene oxide sheets supported on silica as versatile and high-performance adsorbents for solid-phase extraction. *Angew. Chem. Int. Ed.*, **2011**, 123, 6035–6039.
- ¹³ H. J. Choi, N. A. Kumar and J. B. Baek, Graphene supported non-precious metal-macrocycle catalysts for oxygen reduction reaction in fuel cells. *Nanoscale*, **2015**, 7, 6991–6998.
- ¹⁴ M. R. Gao, X. Cao, Q. Gao, Y. F. Xu, Y. R. Zheng, J. Jiang and S. H. Yu, Nitrogen-doped graphene supported CoSe₂ nanobelt composite catalyst for efficient water oxidation, *ACS Nano*, **2014**, 8, 3970–3978.
- 15 X. R. Xia, N. A. Monteiro-Riviere and J. E. Riviere, An index for characterization of nanomaterials in biological systems, *Nat. Nanotech.*, **2010**, 5, 671–675.
- 16 J. Comer, R. Chen, H. Poblete, A. Vergara-Jaque and J. E. Riviere, Predicting adsorption affinities of small molecules on carbon nanotubes using molecular dynamics simulation, *ACS. Nano*, **2015**, 9, 11761–11774.
- 17 R. Chen, Y. T. Zhang, N. A. Monteiro-Riviere and J. E. Riviere, Quantification of nanoparticle pesticide adsorption: computational approaches based on experimental data, *Nanotoxicology*, **2016**, 10, 1118–1128.
- 18 S. Agnihotri, M. J. Rood and M. Rostam-Abadi, Adsorption equilibrium of organic vapors on single-walled carbon nanotubes, *Carbon*, **2005**, 43, 2379–2388.
- 19 A. K. Chopra, M. K. Sharma and S. Chamoli, Bioaccumulation of organochlorine pesticides in aquatic system—an overview, *Environ. Monit. Assess.*, **2011**, 173,

905-916.

- 20 M. Iqbal, J. H. Syed, A. Katsoyiannis, R. N. Malik, A. Farooqi, A. Butt, J. Li, G. Zhang, A. Cincinelli and K. C. Jones, Legacy and emerging flame retardants (FRs) in the freshwater ecosystem: A review, *Environ. Res.*, **2017**, 152, 26–42.
- 21 H. Tang, Y. Zhao, X. N. Yang, D. M. Liu, S. J. Shan, F. Y. Cui and B. S. Xing, Understanding the pH-dependent adsorption of ionizable compounds on graphene oxide using molecular dynamics simulations, *Environ. Sci.: Nano*, **2017**, 4, 1935–1943.
- 22 J. Zhao, Z. Y. Wang, J. C. White and B. S. Xing, Graphene in the aquatic environment: adsorption, dispersion, toxicity and transformation, *Environ. Sci. Technol.*, **2014**, 48, 9995–10009.
- 23 X. X. Chen and B. L. Chen, Macroscopic and spectroscopic investigations of the adsorption of nitroaromatic compounds on graphene oxide, reduced graphene oxide, and graphene nanosheets, *Environ. Sci. Technol.*, **2015**, 49, 6181–6189.
- 24 Z. X. Jin, X. X. Wang, Y. B. Sun, Y. J. Ai and X. K.Wang, Adsorption of 4-n-nonylphenol and bisphenol-A on magnetic reduced graphene oxides: a combined experimental and theoretical studies, *Environ. Sci. Technol.*, **2015**, 49, 9168–9175.
- 25 H. Yan, H. Wu, K. Li, Y. W. Wang, X. Tao, H. Yang, A. M. Li and R. S. Cheng, Influence of the surface structure of graphene oxide on the adsorption of aromatic organic compounds from water, *ACS Appl. Mater. Interfaces*, **2015**, 7, 6690–6697.
- 26 V. C. Sanchez, A. Jachak, R. H. Hurt and A. B. Kane, Biological interactions of

- graphene-family nanomaterials: an interdisciplinary review, *Chem. Res. Toxicol.*, **2012**, 25, 15–34.
- 27 V. Georgakilas, J. N. Tiwari, K. C. Kemp, J. A. Perman, A. B. Bourlinos, K. S. Kim and R. Zboril, Noncovalent functionalization of graphene and graphene oxide for energy materials, biosensing, catalytic, and biomedical applications, *Chem. Rev.*, **2016**, 116, 5464–5519.
- 28 H. Tang, Y. Zhao, X. N. Yang, D. M. Liu, P. H. Shao, Z. G. Zhu, S. J. Shan, F. Y. Cui and B. S. Xing, New insight into the aggregation of graphene oxide using molecular dynamics simulations and extended Derjaguin–Landau–Verwey–Overbeek theory, *Environ. Sci. Technol.*, **2017**, 51, 9674–9682.
- 29 S. Osella, A. Minoia and D. Beljonne, Combined molecular dynamics and density functional theory study of azobenzene–graphene interfaces, *J. Phys. Chem. C.*, **2016**, 120, 6651–6658.
- 30 A. Rissanou and V. Harmandaris, Structure and dynamics of poly(methyl methacrylate)/graphene systems through atomistic molecular dynamics simulations, *J. Nanopart. Res.*, **2013**, 15, 1589.
- 31 L. Y. Xu and X. N. Yang, Molecular dynamics simulation of adsorption of pyrene–polyethylene glycol onto graphene, *J. Colloid. Interf. Sci.*, **2014**, 418, 66–73.
- 32 Y. Wang, J. W. Chen, X. X. Wei, A. J. Hernandez-Maldonado and Z. F. Chen, Unveiling adsorption mechanisms of organic pollutants onto carbon nanomaterials by DFT computations and pp-LFER modeling, *Environ. Sci. Technol.*, **2017**, 51,

- 11820-11828.
- 33 G. R. Famini and L. Y. Wilson, Using theoretical descriptors in linear free energy relationships: characterizing several polarity, acid and basicity scales, *J. Phys. Org. Chem.*, **1999**, 12, 645–653.
- 34 G. R. Famini and L. Y. Wilson, Using theoretical descriptors in quantitative structure activity relationships: application to partition properties of alkyl (1-phenylsulfonyl) cycloalkane-carboxylates, *Chemosphere*, **1997**, 35, 2417–2447.
- 35 A. Baumer, K. Bittermann, N. Klüver and B. I. Escher, Baseline toxicity and ion-trapping models to describe the pH-dependence of bacterial toxicity of pharmaceuticals, *Environ. Sci.: Processes Impacts*, 2017, **19**, 901–916.
- 36 B. I. Escher and R. P. Schwarzenbach, Mechanistic studies on baseline toxicity and uncoupling of organic compounds as a basis for modeling effective membrane concentrations in aquatic organisms, *Aquat. Sci.*, **2002**, 64, 20–35.
- 37 Royal Society of Chemistry. *ChemSpider*; **2017**; http://www.chemspider.com.
- 38 *ChemicalBook*; 2017; https://www.chemicalbook.com/
- 39 K. Vanommeslaeghe, E. Hatcher, C. Acharya, S. Kundu, S. Zhong, J. Shim, E. Darian, O. Guvench, P. Lopes, I. Vorobyov and A. D. Mackerell, Jr., CHARMM general force field: A force field for drug-like molecules compatible with the CHARMM all-atom additive biological force fields, *J. Comput. Chem.*, **2010**, 31, 671–690.
- 40 K. Vanommeslaeghe and A. D. MacKerell, Jr., Automation of the CHARMM General Force Field (CGenFF) I: Bond perception and atom typing, *J. Chem. Inf.*

- Model., 2012, 52, 3144-3154.
- 41 K. Vanommeslaeghe, E. P. Raman and A. D. MacKerell, Jr., Automation of the CHARMM General Force Field (CGenFF) II: Assignment of bonded parameters and partial atomic charges, *J. Chem. Inf. Model.*, **2012**, 52, 3155–3168.
- 42 T. P. Senftle, S. Hong, M. M. Islam, S. B. Kylasa, Y. X. Zheng, Y. K. Shin, C. Junkermeier, R. Engel-Herbert, M. J. Janik, H. M. Aktulga, T. Verstraelen, A. Grama and A. C. T. van Duin, The ReaxFF reactive force-field: development, applications and future directions, *npj. Comp. Mater.*, **2016**, 2, 15011.
- 43 H. M. Aktulga, J. C. Fogarty, S. A. Pandit and A. Y. Grama, Parallel reactive molecular dynamics: Numerical methods and algorithmic techniques, *Parallel*. *Computing.*, **2012**, 38, 245–259.
- 44 S. Plimpton. Fast parallel algorithms for short-range molecular dynamics, *J. Comput. Phys.*, **1995**, 117, 1–19.
- 45 X. R. Xia, N. A. Monteiro-Riviere, S. Mathur, X. Song, L. Xiao, S. J. Oldenberg, B. Fadeel and J. E. Riviere, Mapping the Surface Adsorption Forces of Nanomaterials in Biological Systems, *ACS Nano*, **2011**, 5, 9074–9081.
- 46 J. C. Phillips, R. Braun, W. Wang, J. Gumbart, E. Tajkhorshid, E. Villa, C. Chipot, R. D. Skeel, L. Kale and K. Schulten, Scalable Molecular Dynamics with NAMD, *J. Comput. Chem.*, **2005**, 26, 1781–1802.
- 47 W. L. Jorgensen, J. Chandrasekhar, J. D. Madura, R. W. Impey and M. L. Klein, Comparison of simple potential functions for simulating liquid water, *J. Chem. Phys.*, **1983**, 79, 926–935.

- 48 S. E. Feller, Y. H. Zhang, R. W. Pastor and B. R. Brooks, Constant pressure molecular dynamics simulations: The Langevin piston method, *J. Chem. Phys.*, **1995**, 103, 4613–4621.
- 49 U. Essmann, L. Perera, M. L. Berkowitz, T. Darden, H. Lee and L. G. Pedersen, A smooth particle mesh Ewald method, *J. Chem. Phys.*, **1995**, 103, 8577–8593.
- 50 W. Humphrey, A. Dalke and K. Schulten, VMD Visual molecular dynamics, *J. Mol. Graphics*, **1996**, 14, 33–38.
- 51 E. Darve and A. Pohorille, Calculating free energies using average force, *J. Chem. Phys.*, **2001**, 115, 9169–9183.
- 52 J. Comer, J. C. Gumbart, J. Hénin, T. Lelièvre, A. Pohorille and C. Chipot, The adaptive biasing force method: everything you always wanted to know, but were afraid to ask. *J. Phys. Chem.*, B **2015**, 119, 1129–1151.
- 53 G. Fiorin, M. L. Klein and J. Hénin, Using collective variables to drive molecular dynamics simulations, *Mol. Phys.*, **2013**, 111, 3345–3362.
- 54 Y. Zhao and D. Truhlar, The M06 suite of density functionals for main group thermochemistry, thermochemical kinetics, noncovalent interactions, excited states, and transition elements: two new functionals and systematic testing of four M06-class functionals and 12 other functionals, *Theor. Chem. Acc.*, **2008**, 120, 215–241.
- 55 M. J. Frisch, G. W. Trucks, H. B. Schlegel, G. E. Scuseria, M. A. Robb, J. R. Cheeseman, G. Scalmani, V. Barone, B. Mennucci, G. A. Petersson, H. Nakatsuji, M. Caricato, X. Li, H. P. Hratchian, A. F. Izmaylov, J. Bloino, G. Zheng, J. L.

Sonnenberg, M. Hada, M. Ehara, K. Toyota, R. Fukuda, J. Hasegawa, M. Ishida, T. Nakajima, Y. Honda, O. Kitao, H. Nakai, T. Vreven, J. A. Montgomery, Jr. J. E. Peralta, F. Ogliaro, M. Bearpark, J. J. Heyd, E. Brothers, K. N. Kudin, V. N. Staroverov, R. Kobayashi, J. Normand, K. Raghavachari, A. Rendell, J. C. Burant, S. S. Iyengar, J. Tomasi, M. Cossi, N. Rega, J. M. Millam, M. Klene, J. E. Knox, J. B. Cross, V. Bakken, C. Adamo, J. Jaramillo, R. Gomperts, R. E. Stratmann, O. Yazyev, A. J. Austin, R. Cammi, C. Pomelli, J. W. Ochterski, R. L. Martin, K. Morokuma, V. G. Zakrzewski, G. A. Voth, P. Salvador, J. J. Dannenberg, S. Dapprich, A. D. Daniels, O. Farkas, J. B. Foresman, J. V. Ortiz, J. Cioslowski and D. J. Fox, Gaussian 09, Revision A. 01; Gaussian, Inc.: Wallingford CT, 2009.

- 56 W. R. Wadt and P. J. Hay, Ab initio effective core potentials for molecular calculations. Potentials for main group elements Na to Bi, *J. Chem. Phys.*, **1985**, 82, 284–298.
- 57 Talete srl, 2012. Dragon (Software for Molecular Descriptor Calculation) Version 6.0. http://www.talete.mi.it/.
- 58 J. S. Murray, P. Politzer and G. R. Famini, Theoretical alternatives to linear solvation energy relationships, *J. Mol. Struct.-Theochem*, **1998**, 454, 299–306.
- 59 L. Y. Wilson and G. R. Famini, Using theoretical descriptors in quantitative structure-activity relationships: some toxicological indices, *J. Med. Chem.*, **1991**, 34, 1668-1674.
- 60 A. Golbraikh, M. Shen, Z. Y. Xiao, Y. D. Xiao, K. H. Lee and A. Tropsha,

Rational selection of training and test sets for the development of validated QSAR models, *J. Comput. Aided. Mol. Des.*, **2003**, 17, 241–253.

61 O. G. Apul, Q. L. Wang, T. Shao, J. R. Rieck and T. Karanfil, Predictive model development for adsorption of aromatic contaminants by multi-walled carbon nanotubes, *Environ. Sci. Technol.*, **2013**, 47, 2295–2303.